# Line intensities for x-ray emission in Mg$^{12+}$ collisions with H and He atoms

## M R Fogle and M S Pindzola[1]

Department of Physics, Auburn University, Auburn, AL, United States of America

E-mail: pindzola@physics.auburn.edu

### Abstract

State selective charge transfer cross sections are calculated in Mg$^{12+}$ collisions with H and He atoms at incident energies of 1.0, 3.0, and 5.0 keV amu$^{-1}$ using a time-dependent lattice method. Total capture cross sections using the time-dependent lattice method are found to be larger than those previously calculated using the Landau–Zener method. Lyman line ratios are calculated using the time-dependent lattice capture cross sections and standard radiative transitions for both the H and He atoms. Lyman line probabilities are presented for both H and He. The strongest probability for both H and He is the Lyman $\alpha$ emission, but relatively strong probabilities for He at an incident energy of 1.0 keV amu$^{-1}$ are found for Lyman $\beta$, $\gamma$, $\delta$, and $\epsilon$ emission.

Keywords: collisions, x-ray, intensities

(Some figures may appear in colour only in the online journal)

## 1. Introduction

The charge transfer interaction of solar wind ions with interstellar and planetary atoms, and even cometary and atmospheric molecules, presents one of the predominant atomic interactions that drives observed emission [1, 2]. The resulting emission lines due to captured electrons provides information about the interaction environment, examples are temperature, density, and relative ion abundance. Predicting the resulting emission subsequent to charge transfer requires knowledge of the state-selective ($nl$) charge transfer cross sections, typically on the order of $10^{-15}$ cm$^2$. While there is a considerable body of knowledge, both experimental and theoretical, regarding various charge transfer ion-atom partners at various interaction energies, much of this work is focussed on an energy regime above the nominal interaction energies associated with solar wind interactions, that is less than 10.0 keV amu$^{-1}$.

In this lower interaction energy regime, several theoretical methods have been employed to fill the void of lacking and/or sparse charge transfer cross section data needs for modeling and analysis of observations. Some of the more predominant methods are classical trajectory Monte Carlo (CTMC) [3], multichannel Landau–Zener (MCLZ) [4, 5], and

atomic orbital (or molecular orbital) close-coupling (AOCC, MOCC) [6, 7]. These methods are typically employed over specific interaction energy ranges, with CTMC and MCLZ at higher energies and AOCC/MOCC at lower energies. The CTMC and MCLZ methods are not as computationally expensive as the AOCC and MOCC methods. It should be noted that at the lower interaction energies, transfer ionization, stabilized double capture, and double capture autoionization can contribute to the total charge transfer cross section. These processes are rarely included in models.

In making charge transfer cross section calculations, it is not straightforward which method to choose that optimizes accuracy, computational complexity, and time. Several of these models have been shown to provide accurate cross sections for a given ion-atom interaction pair at a given energy, while displaying divergent results for a different interaction pair at the same energy. It should also be noted that these methods primarily calculate the principal quantum state, $n$, of the captured electron and do not inherently calculate the angular momentum quantum state, $l$, which is the primary driver in the resulting emission cascade. The most prolific $l$-distributions used in conjunction with these models to determine $nl$ cross sections are the statistical:

$$W_{nl}^{st} = \frac{(2l+1)}{n^2} \tag{1}$$

---

[1] Author to whom any correspondence should be addressed.

and the low-energy distribution [8, 9]:

$$W_{nl}^{le} = \frac{(2l+1)(n-l)!^2}{(n+1)!(n-1-l)!}. \qquad (2)$$

The statistical distribution function is typically used for interaction energies of 5–10 keV amu$^{-1}$. Below this energy range the low-energy distribution is preferred.

The time-dependent lattice method is based on following the time-dependent interaction of the bare ion and the atom on a three dimensional spatial lattice. The large number of mesh points needed are partitioned over the cores on a massively parallel computer. The time-dependent lattice method has been used in the past to directly calculate $nl$ charge transfer cross sections for Be$^{4+}$ on H [10], C$^{6+}$ on H and He [11], and O$^{8+}$ on H and He [12]. In this paper the time-dependent lattice method is used to calculate the $nl$ charge transfer cross sections for Mg$^{12+}$ on H and He atoms at interaction energies of 1.0, 3.0, and 5.0 keV amu$^{-1}$. The resulting $nl$ capture cross sections are then used in a dipole-allowed cascade model [11, 12] to determine the relative Lyman emission line intensities and ratios typically needed in plasma diagnostics.

The time-dependent lattice method is reviewed in section 2, capture cross sections are presented in section 3.1, emission line ratios and emission probabilities are shown in section 3.2, and a brief review is found in section 4. Unless otherwise stated, we will use atomic units.

## 2. Theory

For bare ion collisions with atoms the time-dependent Schrodinger equation, in the frame of reference of the stationary Mg$^{12+}$ ion, is given by:

$$i\frac{\partial P(x, y, z, t)}{\partial t} = (-\frac{1}{2}\nabla^2 - \frac{12.0}{r})P(x, y, z, t)$$
$$+ W(x, y, z, t)P(x, y, z, t). \qquad (3)$$

For the moving H atom:

$$W(x, y, z, t) = -\frac{1}{R(t)}, \qquad (4)$$

where the active electron interacts with the H$^+$ core. For the moving He atom:

$$W(x, y, z, t) = -\frac{1}{R(t)} - \frac{(1 + (1.665)R(t))e^{-(3.36)R(t)}}{R(t)}, \qquad (5)$$

where the active electron interacts with the He$^+$ core through a model potential [13]. For straight line trajectories:

$$R(t) = \sqrt{(x-b)^2 + (y - (y_0 + vt))^2 + z^2}, \qquad (6)$$

where $b$ is an impact parameter, $y_0 < 0$ is a starting position, and $v$ is the projectile speed.

The initial wavefunction for the solution of the time-dependent Schrodinger equation of equation (3) is given by:

$$P(x, y, z, t = 0) = P_{1s0}(x, y, z), \qquad (7)$$

where $P_{1s0}(x, y, z)$ is the ground state of the moving H or He atom. The asymptotic wavefunction, $P(x, y, z, t \rightarrow \infty)$, is obtained by propagating the time-dependent Schrodinger equation of equation (3) until the projectile has moved well past the target. The probability of capture is given by:

$$C_{nlm}(v, b) = |\int_{-\infty}^{\infty} dx \int_{-\infty}^{\infty} dy$$
$$\times \int_0^{\infty} dz P_{nlm}^*(x, y, z)P(x, y, z, t \rightarrow \infty)|^2, \qquad (8)$$

where $P_{nlm}(x, y, z)$ are ground and excited states of the stationary Mg$^{12+}$ ion. The $nl$ subshell capture cross section for a specific velocity is given by:

$$\sigma_{nl} = 2\pi \sum_m \int_0^{\infty} bC_{nlm}(v, b)db. \qquad (9)$$

The $n$ capture cross sections are found by summing $\sigma_{nl}$ over $n$, while the $l$ capture cross sections are found by summing $\sigma_{nl}$ over $l$.

## 3. Results

Time-dependent lattice calculations for Mg$^{12+}$ collisions with H and He atoms are carried out at incident energies of 1.00, 3.00, and 5.00 keV amu$^{-1}$. An $(x, y, z)$ lattice used $720 \times 720 \times 360$ points with a uniform grid spacing of $\delta x = \delta y = \delta z = 0.10$. The lattice extends from $-36.0$ to $+36.0$ in the x and y directions and from $0.0$ to $+36.0$ in the z direction. For each incident energy, calculations were carried out at 70 impact parameters ranging from $b = 0.10$ to $b = 20.0$. Each of the 210 time-dependent lattice calculations for the H and He atoms were carried out on the $(x, y, z)$ lattice partitioned over $24 \times 24 \times 12$ cores on a massively parallel computer.
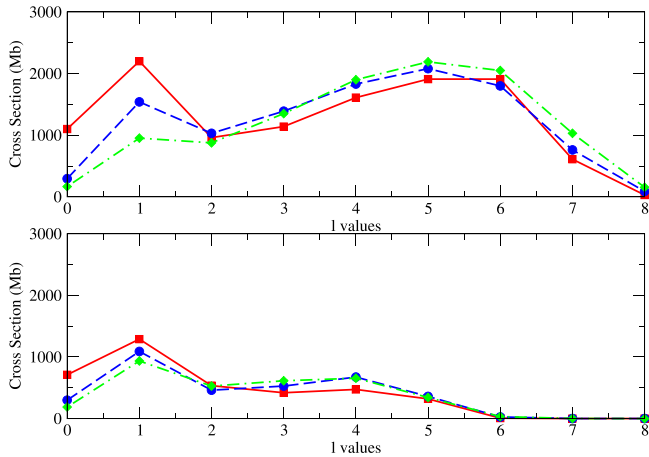
### 3.1. Capture cross sections

The capture cross sections from equation (9) as a function of $n$ for both the H and He atoms are presented in figure 1. The capture cross section for H peaks at $n = 7$ with a value of 6640 Mb at 1.0 keV amu$^{-1}$. The capture cross section for He peaks at $n = 5$ with a value of 1920 Mb and at $n = 6$ with a value of 1740 Mb, both at 1.0 keV amu$^{-1}$.

The capture cross sections from equation (9) as a function of $l$ for the H and He atoms are presented in figure 2. The capture cross section for H peaks at $l = 1$ with a value of 2200 Mb and at $l = 5, 6$ with values of 1919 Mb, all at 1.0 keV amu$^{-1}$. The capture cross section for He peaks at $l = 1$ with 1290 Mb at 1.0 keV amu$^{-1}$.

The capture cross sections from equation (9) as a function of $nl$ ($5s - 9k$) for the H atom are presented in table 1. At 1.0 keV amu$^{-1}$ the largest cross section is for $7p$ with a value of 1490 Mb, at 3.0 keV amu$^{-1}$ the largest cross section is for $7h$ with a value of 1320 Mb, and at 5.0 kev amu$^{-1}$ the largest cross section is for $7h$ and $7i$, both at 1320 Mb.
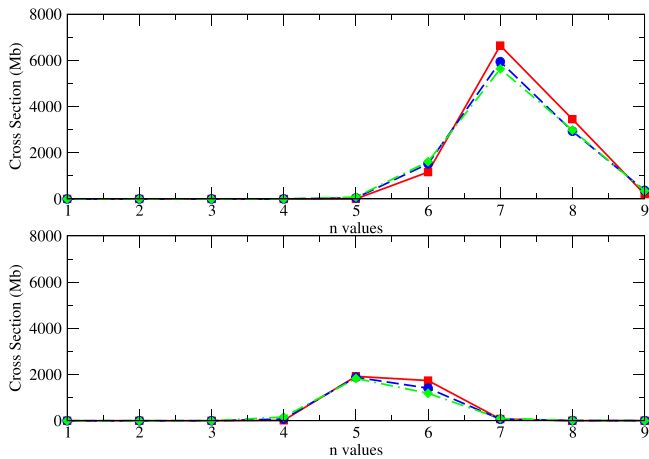
**Figure 1.** Mg$^{12+}$ charge transfer. Top graph: H atom target, solid line squares (red): 1.0 keV amu$^{-1}$, dashed line circles (blue): 3.0 keV amu$^{-1}$, dot dashed line diamonds (green): 5.0 keV amu$^{-1}$. Bottom graph: He atom target, solid line squares (red): 1.0 keV amu$^{-1}$, dashed line circles (blue): 3.0 keV amu$^{-1}$, dot dashed line diamonds (green): 5.0 keV amu$^{-1}$. (1.0 Mb = $1.0 \times 10^{-18}$ cm$^2$.)



**Figure 2.** Mg$^{12+}$ charge transfer. Top graph: H atom target, solid line squares (red): 1.0 keV amu$^{-1}$, dashed line circles (blue): 3.0 keV amu$^{-1}$, dot dashed line diamonds (green): 5.0 keV amu$^{-1}$. Bottom graph: He atom target, solid line squares (red): 1.0 keV amu$^{-1}$, dashed line circles (blue): 3.0 keV amu$^{-1}$, dot dashed line diamonds (green): 5.0 keV amu$^{-1}$. (1.0 Mb = $1.0 \times 10^{-18}$ cm$^2$.)

The capture cross sections from equation (9) as a function of $nl$ ($4s-7i$) for the He atom are presented in table 2. At 1.0 keV amu$^{-1}$ the largest cross section if for $6p$ with a value of 684 Mb, at 3.0 keV amu$^{-1}$ the largest cross section is for $6g$ with a value if 384 Mb, and at 5.0 keV amu$^{-1}$ the largest cross section is for $5f$ with a value of 348 Mb.

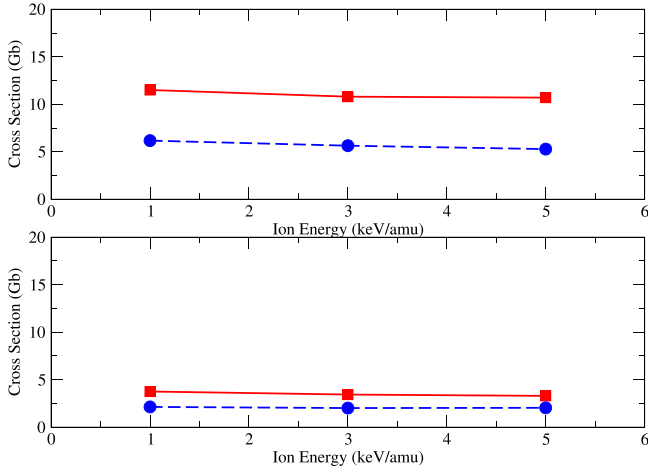The total capture cross sections for the H and He atoms are presented in figure 3. The total capture cross section for the H atom at 1.0 keV amu$^{-1}$ is 11.5 Gb, at 3.0 keV amu$^{-1}$ is 10.8 Gb, and at 5.0 keV amu$^{-1}$ is 10.7 Gb. The total capture cross section for the He atom at 1.0 keV amu$^{-1}$ is 3.76 Gb, at 3.0 keV amu$^{-1}$ is 3.44 Gb, and at 5.0 keV amu$^{-1}$ is 3.30 Gb. The total capture cross sections from 1.0 keV amu$^{-1}$ to

**Table 1.** Mg$^{12+}$ + H collision cross sections in $1.0 \times 10^{-18}$ cm$^2$.

| $n$ | $l$ | 1.0 keV amu$^{-1}$ | 3.0 keV amu$^{-1}$ | 5.0 keV amu$^{-1}$ |
|---|---|---|---|---|
| 5 | 0 | 2 | 22 | 19 |
|   | 1 | 0 | 7 | 25 |
|   | 2 | 0 | 10 | 13 |
|   | 3 | 0 | 6 | 14 |
|   | 4 | 0 | 3 | 10 |
| 6 | 0 | 708 | 165 | 79 |
|   | 1 | 128 | 554 | 365 |
|   | 2 | 107 | 232 | 248 |
|   | 3 | 78 | 223 | 296 |
|   | 4 | 78 | 206 | 333 |
|   | 5 | 58 | 142 | 292 |
| 7 | 0 | 371 | 99 | 58 |
|   | 1 | 1490 | 814 | 461 |
|   | 2 | 559 | 624 | 488 |
|   | 3 | 738 | 907 | 810 |
|   | 4 | 1080 | 1220 | 1180 |
|   | 5 | 1210 | 1320 | 1320 |
|   | 6 | 1190 | 954 | 1320 |
| 8 | 0 | 13 | 7 | 9 |
|   | 1 | 564 | 158 | 95 |
|   | 2 | 282 | 151 | 117 |
|   | 3 | 312 | 236 | 210 |
|   | 4 | 434 | 380 | 360 |
|   | 5 | 616 | 580 | 549 |
|   | 6 | 671 | 768 | 681 |
|   | 7 | 554 | 650 | 963 |
| 9 | 0 | 1 | 1 | 1 |
|   | 1 | 18 | 7 | 6 |
|   | 2 | 12 | 9 | 10 |
|   | 3 | 13 | 13 | 15 |
|   | 4 | 12 | 23 | 20 |
|   | 5 | 21 | 41 | 31 |
|   | 6 | 45 | 74 | 48 |
|   | 7 | 56 | 111 | 64 |
|   | 8 | 29 | 89 | 154 |

**Table 2.** Mg$^{12+}$ + He collision cross sections in $1.0 \times 10^{-18}$ cm$^2$.

| $n$ | $l$ | 1.0 keV amu$^{-1}$ | 3.0 keV amu$^{-1}$ | 5.0 keV amu$^{-1}$ |
|---|---|---|---|---|
| 4 | 0 | 15 | 39 | 68 |
|   | 1 | 0 | 9 | 30 |
|   | 2 | 1 | 15 | 43 |
|   | 3 | 1 | 9 | 20 |
| 5 | 0 | 669 | 244 | 111 |
|   | 1 | 592 | 792 | 727 |
|   | 2 | 305 | 285 | 340 |
|   | 3 | 170 | 280 | 348 |
|   | 4 | 185 | 282 | 308 |
| 6 | 0 | 27 | 16 | 9 |
|   | 1 | 684 | 285 | 173 |
|   | 2 | 220 | 156 | 138 |
|   | 3 | 234 | 232 | 235 |
|   | 4 | 268 | 384 | 322 |
|   | 5 | 305 | 336 | 315 |
| 7 | 0 | 0 | 0 | 0 |
|   | 1 | 11 | 5 | 5 |
|   | 2 | 9 | 3 | 6 |
|   | 3 | 14 | 4 | 10 |
|   | 4 | 20 | 6 | 23 |
|   | 5 | 15 | 23 | 24 |
|   | 6 | 7 | 25 | 28 |

J. Phys. B: At. Mol. Opt. Phys. **53** (2020) 095203

M R Fogle and M S Pindzola



**Figure 3.** $Mg^{12+}$ charge transfer. Top graph: H atom target, solid line squares (red): time-dependent lattice method, dashed line circles (blue): Landau–Zener method. Bottom graph: He atom target, solid line squares (red): time-dependent lattice method, dashed line circles (blue): Landau–Zener method. ($1.0 \, Gb = 1.0 \times 10^{-15} \, cm^2$).

$5.0 \, keV \, amu^{-1}$ calculated using an approximate MCLZ method [14] are found to be almost a factor of 2 smaller than the time-dependent lattice cross sections.

### 3.2. Emission probabilities

For population of the n shells in $Mg^{12+}$ collisions with the H and He atoms, the probabilities of Lyman line emission, considering only dipole-allowed transitions, are given by:

$$P(\alpha) = \sum_{n=2}^{9} \frac{\sigma_n B_{\alpha n}}{\sigma_t}$$

$$P(\beta) = \sum_{n=3}^{9} \frac{\sigma_n B_{\beta n}}{\sigma_t}$$

$$P(\gamma) = \sum_{n=4}^{9} \frac{\sigma_n B_{\gamma n}}{\sigma_t}$$

$$P(\delta) = \sum_{n=5}^{9} \frac{\sigma_n B_{\delta n}}{\sigma_t}$$

$$P(\epsilon) = \sum_{n=6}^{9} \frac{\sigma_n B_{\epsilon n}}{\sigma_t}$$

$$P(\zeta) = \sum_{n=7}^{9} \frac{\sigma_n B_{\zeta n}}{\sigma_t}, \tag{10}$$

where the total capture cross section, $\sigma_t$, is found by summing $\sigma_{nl}$ over $nl$. Expressions for the $B$ coefficients involve cross section ratios and radiative rate ratios. For example

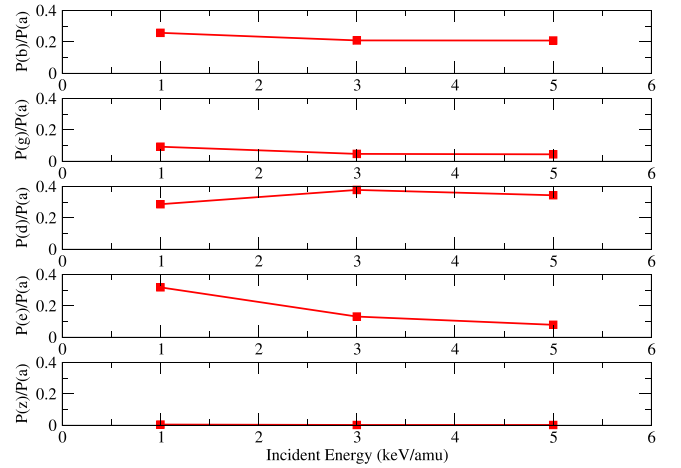$$B_{\beta 3} = \frac{\sigma_{3p}}{\sigma_3} \frac{A(3p \rightarrow 1s)}{A_t(3p)}, \tag{11}$$

where

$$A_t(nl) = \sum_{n'l'} A(nl \rightarrow n'l'). \tag{12}$$

Expressions for hign $n$ become quite involved. Lyman probability ratios for the H and He atoms are presented in figures 4 and 5. We note that the $P(\gamma)/P(\alpha)$ and $P(\delta)/P(\alpha)$
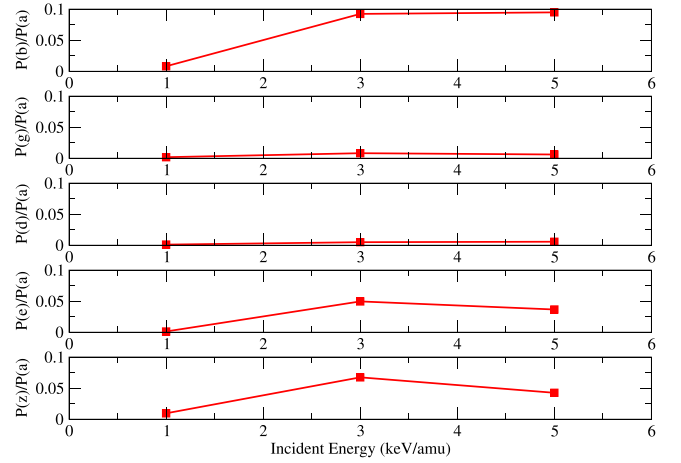


**Figure 4.** Lyman line ratios for $Mg^{12+}$ + H collisions solid line squares (red): time-dependent lattice method.



**Figure 5.** Lyman line ratios for $Mg^{12+}$ + He collisions solid line squares (red): time-dependent lattice method.

ratios are small for $Mg^{12+}$ + H collisions, while the $P(\zeta)/P(\alpha)$ ratio is small for $Mg^{12+}$ + He collisions.

Setting the $P(\alpha)$ probability to a relative intensity of 1.0, the other $P(\beta)$, $P(\gamma)$, $P(\delta)$, $P(\epsilon)$, and $P(\zeta)$ probabilities are plotted as a function of photon energy for the H and He atoms in figures 6 and 7. The emission spectrum is convoluted to represent a 10 eV FWHM detection resolution. The Lyman lines are at 1471 eV ($\alpha$), 1745 eV ($\beta$), 1840 eV ($\gamma$), 1884 eV ($\delta$), 1908 eV ($\epsilon$), and 1923 eV ($\zeta$). For $Mg^{12+}$ + H collisions in figure 6, the Lyman ($\beta$), Lyman ($\epsilon$), and Lyman ($\zeta$) lines begin to emerge at 3.0 and 5.0 keV amu$^{-1}$. For $Mg^{12+}$ + He collisions in figure 7, the Lyman ($\beta$), Lyman ($\delta$), and Lyman ($\epsilon$) lines are visible at all the ion energies.

## 4. Summary

State selective charge transfer cross sections were calculated in $Mg^{12+}$ collisions with H and He atoms using a time-dependent lattice method. Calculations were carried out at incident energies of 1.0, 3.0, and 5.0 keV amu$^{-1}$, and

J. Phys. B: At. Mol. Opt. Phys. 53 (2020) 095203

M R Fogle and M S Pindzola
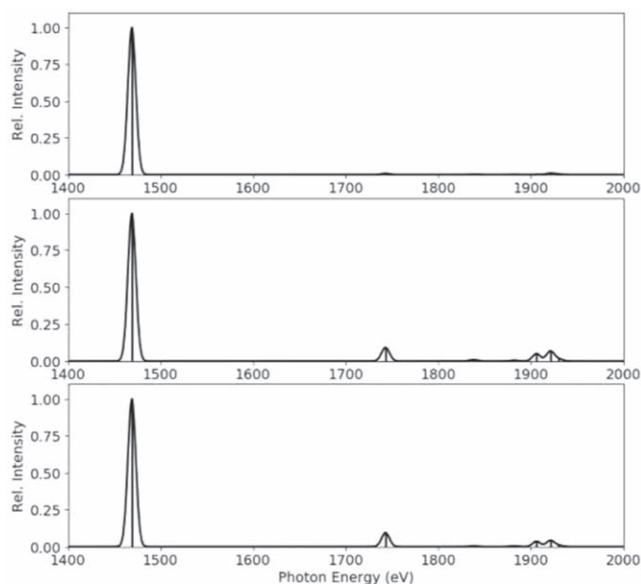


**Figure 6.** Lyman probabilities as a function of photon energy (eV) for $Mg^{12+}$ + H collisions. Top graph: $1.0\,keV\,amu^{-1}$ ion energy, middle graph: $3.0\,keV\,amu^{-1}$ ion energy, and bottom graph: $5.0\,keV\,amu^{-1}$ ion energy.
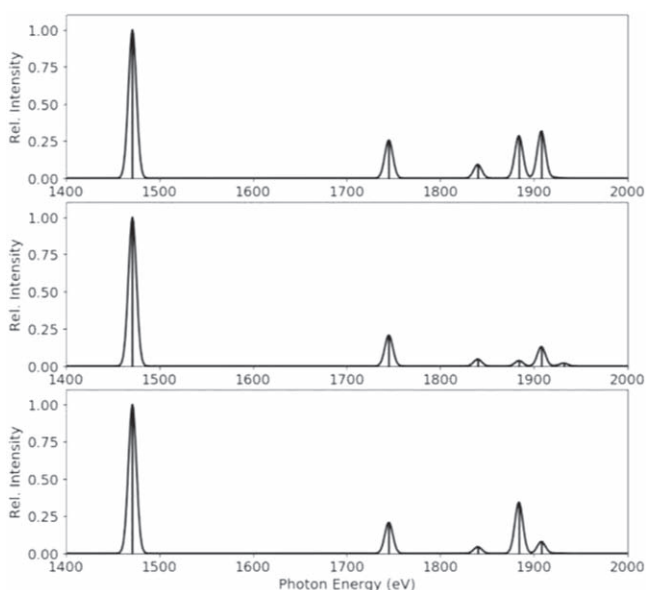


**Figure 7.** Lyman probabilities as a function of photon energy (eV) for $Mg^{12+}$ + He collisions. Top graph: $1.0\,keV\,amu^{-1}$ ion energy, middle graph: $3.0\,keV\,amu^{-1}$ ion energy, and bottom graph: $5.0\,keV\,amu^{-1}$ ion energy.

included $nl$ subshell capture states from $1s$ to $9k$. The total capture cross sections at the three ion energies were found to be larger than the MCLZ calculations [14]. Emission probabilities were then calculated for Lyman lines considering only dipole-allowed transitions. For the H atom the Lyman $\alpha$ probability dominates at low ion energies with the appearance of Lyman $\beta$, $\epsilon$, and $\zeta$ at the higher energies. For the He atom the Lyman $\alpha$, $\beta$, $\delta$, and $\epsilon$ are visible at all the ion energies.

In the future we plan to use the time-dependent lattice method to calculate bare ion collisions with H and He atoms in support of Clemson University Electron Beam Ion Trap experiments. We also will look at bare ion collisions with $H_2$.

## Acknowledgments

## ORCID iDs

M S Pindzola ⓘ https://orcid.org/0000-0001-6787-9249

## References

[1] Lisse C M 1996 *Science* **274** 205
[2] Cravens T E 1997 *Geophys. Res. Lett.* **24** 105
[3] Simcic J, Schultz D R, Mawhorter R J, Cadez I, Greenwood J B, Chutjian A, Liesse C M and Smith S J 2010 *Phys. Rev.* A **81** 062715
[4] Butler S E and Dalgarno A 1980 *Astrophys. J.* **24** 838
[5] Janev R K, Belic D S and Brandsden B H 1983 *Phys. Rev.* A **1293** 28
[6] Kimura M and Olson R E 1984 *J. Phys.* B **17** L713
[7] Fritsch W and Lin C D 1986 *J. Phys.* B **19** 2683
[8] Abramov V A, Baryshnikov F F and Lisitsa V S 1977 *Sov. Phys.—JETP* **47** 469
[9] Krasnopolsky V A, Greenwood J B and Stancil P C 2004 *Space. Sci. Rev.* **113** 271
[10] Minami T, Pindzola M S, Lee T G and Schultz D R 2006 *J. Phys. B: At. Mol. Opt. Phys.* **39** 2877
[11] Pindzola M S and Fogle M 2015 *J. Phys. B: At. Mol. Opt. Phys.* **48** 205203
[12] Pindzola M S, Fogle M and Stancil P C 2018 *J. Phys. B: At. Mol. Opt. Phys.* **51** 065204
[13] Jain A, Lin C D and Fritsch W 1987 *Phys. Rev.* A **36** 2041
[14] Lyons D, Cumbee R S and Stancil P C 2017 *Astrophys. J. Suppl. Ser.* **232** 27